Chemical Physics Letters 491 (2010) 109–122

Contents lists available at ScienceDirect

Chemical Physics Letters

journal homepage: www.elsevier.com/locate/cplett

FRONTIERS ARTICLE

Fundamentals of energy transport, energy conversion, and thermal properties in organic–inorganic heterojunctions

Jonathan A. Malen [a,b], Shannon K. Yee [a], Arun Majumdar [a,c,d], Rachel A. Segalman [c,e,*]

[a] Department of Mechanical Engineering, University of California, Berkeley, CA 94720, USA
[b] Department of Mechanical Engineering, Carnegie Mellon University, Pittsburgh, PA 15213, USA[1]
[c] Material Science Division, Lawrence Berkeley National Laboratory, Berkeley, CA 94720, USA
[d] US Department of Energy, 1000 Independence Ave S.W., Washington, DC 20585, USA[2]
[e] Department of Chemical Engineering, University of California, Berkeley, CA, USA

ARTICLE INFO

Article history:
Received 4 February 2010
In final form 9 March 2010
Available online 19 March 2010

ABSTRACT

Hybrid devices built from organic and inorganic moieties are being actively researched as replacements for inorganic electronics, thermoelectrics, and photovoltaics. However, energy transport and conversion, at the organic–inorganic interface is not well understood. One approach to study this interface is to look at the smallest hybrid building block – the heterojunction of a single organic molecule with inorganic contacts. We present a review of this work, focused on fundamental transport properties of metal–molecule–metal junctions that are related to thermoelectric energy conversion, i.e., electronic conductance, thermopower, and thermal conductance. We describe the motives, strategies, and future directions for considering heterojunctions as building blocks for thermoelectric materials.

1. Introduction and historical overview

Hybrid devices and materials built from organic and inorganic moieties can be designed to combine the complementary strengths of the distinct materials systems. At the organic–inorganic interface unique energy landscapes, nonexistent in the separate components, materialize as the discrete orbitals in the organic are combined with the continuum states in the inorganic. Transport of electricity and heat across these interfaces define the performance of several emergent technologies, including organic transistors, photovoltaics, and light emitting diodes Fig. 1 shows recent work on these technologies as well as newly developed hybrid materials [1–3]. While devices are generally built from ensembles of inorganic-molecule heterojunctions, it is extremely difficult to probe the interfacial structure and properties in this very complex arrangement. Instead, valuable insight can be obtained by studying one or a few junctions at a time. Such single or finite numbered molecular heterojunctions have been extensively studied for molecular electronics, and more recently considered for thermoelectricity. We herein present a review of recent transport studies, centered on the implications of thermopower in molecular junctions as a diagnostic tool and as an energy conversion technology.

Aviram and Ratner's revolutionary suggestion that molecules could behave as electronic circuit components sparked vast experimental and theoretical study of electronic transport in molecular junctions [4]. While a large number investigations of molecules in solution were inspired by this work [5] the experimental ability to investigate individual molecular junctions in solid state lagged theory until 1997, when Reed demonstrated the first single-molecule conductance measurement on an Au–phenyldithiol–Au (Au–PDT–Au) junction [6]. Since then, experiment and theory have begun to converge, though single-molecule devices remain elusive because inelastic effects confound efficient exchange of information [7]. This complicates molecular interconnects and is even more challenging to sophisticated circuit components like switches, logic gates, and transistors. Nonetheless, the scientific community seeks understanding of single-molecule junction electronic transport processes for the design and optimization of ensemble based organic electronics. Electronic conductance is the most studied transport property, but other transport properties, such as thermopower, offer complimentary insight to the transport process. Recent studies of single molecule thermopower have answered open questions about the nature of charge transport, and furthermore, launched a new direction for thermoelectric energy conversion [8].

Thermoelectric materials directly convert thermal energy into electricity. Today's thermoelectrics are primarily used for niche energy conversion applications wherein reliability is paramount and complicated moving parts cannot be tolerated. If the efficiency of thermoelectric energy conversion can be enhanced and materials costs reduced, it holds great promise for scavenging waste heat

* Corresponding author at: Department of Chemical Engineering, University of California, Berkeley, CA, USA.
E-mail address: segalman@berkeley.edu (R.A. Segalman).
[1] Present address.
[2] Present address.

0009-2614/$ - see front matter © 2010 Elsevier B.V. All rights reserved.
doi:10.1016/j.cplett.2010.03.028

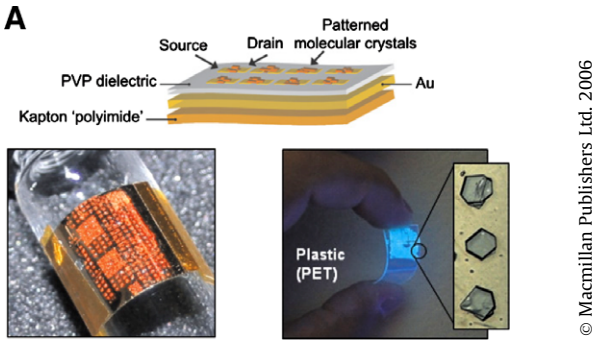

Fig. 1. Organic–inorganic hybrid devices and materials. (A) Organic electronic device architectures contain many organic–inorganic hybrid interfaces. Adapted by permission from Nature, Briseno et al. [1].

(B) Organic light emitting diodes can be used to make thin and flexible displays. Adapted by permission from Nature, Forrest [2].

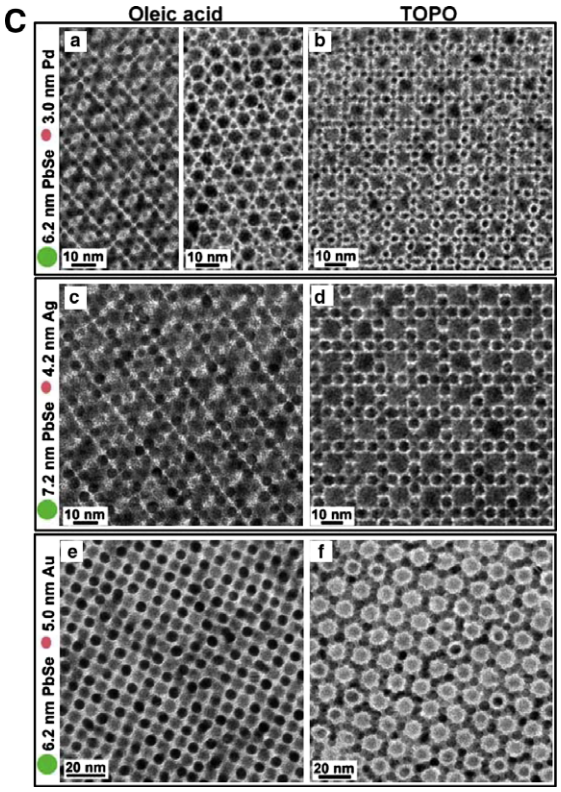

(C) Hyrbid materials are also controlled by transport at the organic–inorganic interface. Shown are TEM images of self-assembled binary superlattices of inorganic nanocrystals coated with either oleic acid or TOPO ligand groups. Adapted by permission from Nature, Shevchenko et al. [3].

in cogeneration schemes or as an active insulation component. Thermoelectric efficiency depends on a combination of material properties, quantified by the thermoelectric figure of merit $ZT = S^2\sigma T/k$, where S is thermopower (a.k.a. Seebeck coefficient measured in volts/degree K), σ is electronic conductivity, and k is thermal conductivity. The best efficiency in thermoelectric energy conversion can be achieved if charge transport occurs through a single energy level [9,10]. Single level transport is, however, difficult to realize in bulk materials. Organic–inorganic heterojunctions are ideal in this regard because they (i) provide transport through discrete molecular orbitals and (ii) have very low vibrational heat conductance because of large mismatch of vibrational spectra between the bulk metal and individual molecules [11]. The thermoelectric figure of merit can be rewritten for molecular junctions as, $ZT = S^2G_eT/G_{Th}$, where G_e and G_{Th} are the junction electronic and thermal conductances. Within this article; we not only discuss the value of thermopower as a diagnostic tool, but also its direct relationship with energy generation.

Isolated molecules have discrete energy levels that can be calculated accurately using computational quantum chemistry. The highest occupied molecular orbital (HOMO) and lowest unoccupied molecular orbital (LUMO) are termed the frontier orbitals because they are most free to participate in chemical reactions. Not surprisingly, the HOMO and LUMO are also the orbitals responsible for transport when a junction is formed, as illustrated in Fig. 2B. In contrast, crystalline inorganic materials have a continuum of electronic energy levels that form a band structure. When a junction is formed between the metal and the molecule, the molecular orbitals mix with the continuum states in the metal to create a junction density of states that has peaks related to the HOMO and LUMO energies. Transport of charge or energy across these unique structures defines transport in hybrid devices and materials.

Over the past decade, significant progress has been made to isolate and experimentally measure electronic transport in molecular junctions. Conductance and $I - V$ characteristics of self-assembled monolayers (SAMs) and single-molecule junctions have been extensively studied. As will be discussed in more detail later, great insight into the structure-conductance property relationships was derived from these SAM experiments [7,12–14]. On the other hand,

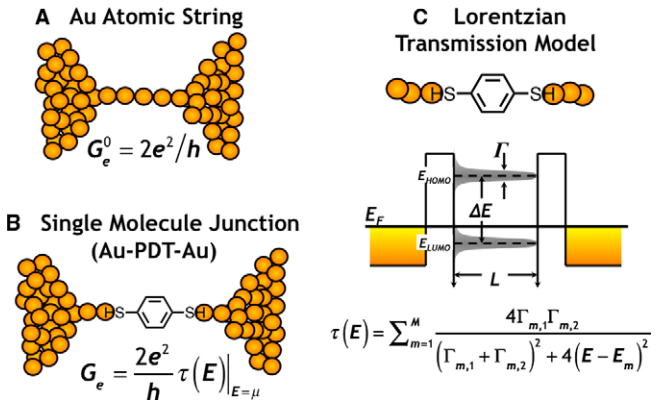

Fig. 2. Schematics of nanoscale junctions. (A) A one-dimensional Au atomic string exhibits a conductance of G_e^0. (B) A Au–PDT–Au molecular junction exhibits a conductance reduced from G_e^0 by a factor of $\tau(E)|_{E=\mu}$. (C) The simple two barrier model is an approximate description of the quasi bound states of a molecular junction.

several additional questions were exposed by SAM studies, including: (a) What molecular orbital dominates transport? (b) How are coupling and alignment of this orbital with contact states related to transport? and (c) What is the origin of observed transport variations? This article focuses on recent contributions to understanding the transport and conversion of energy in molecular junctions. We will particularly focus on the combination of conductance and thermopower measurements and predictions which can lead to significant insight towards molecular transport. We further consider the implications towards efficient thermoelectric energy conversion.

2. Fundamentals of quantum transport

Transport of charge through molecular junctions can be described with the Landauer formalism. In the Landauer picture of transport, charge carriers transmit from one contact, through the molecular junction, and into the opposing contact with an energy-dependant probability defined by the transmission function $\tau(E)$. The Landauer formalism considers only elastic scattering mechanisms, leading to coherent conductance, which is appropriate for short molecules. Inelastic scattering is expected to play a more critical role when the traversal time of the electron is similar to the vibration periods of the molecule [7]. The following sections review the Landauer picture of transport, and its application to electronic conductance, thermopower, and thermal conductance in molecular junctions.

2.1. Quantum of electronic conductance

A fundamental limit in electronic conductance applies even to ideal channels in the absence of elastic scattering mechanisms. This is best demonstrated by considering a one-dimensional string of atoms, as shown in Fig. 2A. The positive current from contact 1 to contact 2, I_{1-2}, is defined as

$$I_{1-2} = \int_{-\infty}^{\infty} (f_1 - f_2) e v D(E) dE, \tag{1}$$

where f_1 and f_2 are the equilibrium occupation probabilities of electrons in contacts 1 and 2 (for metallic contacts these are Fermi distributions $f_i = (1 + e^{(E-\mu_i)/k_B T_i})^{-1}$), e is the positive unit of charge, v is the velocity of the flowing electrons, $D(E)$ is the density of electronic states in the channel, and dE is a small energy interval. For the zero temperature case, when a small positive voltage difference exists between contact 1 and contact 2, V_{1-2}, the difference between f_1 and f_2 is

$$f_1 - f_2 = eV_{1-2}\left(-\left.\frac{df}{dE}\right|_{E=\mu}\right) = eV_{1-2}\delta(E-\mu). \tag{2}$$

The above approximation makes use of the fact that $-df/dE$ demonstrates properties of a Dirac-delta function as the temperature tends towards 0 K. In a one-dimensional, non-scattering wire, the density of states is inversely proportional to the group velocity of the electron, $D(E) = 2/hv$. When this expression for $D(E)$ and Eq. (2) are substituted into Eq. (1), a statement of Ohm's law results

$$I_{1-2} = \frac{2e}{h}\int_{-\infty}^{\infty}(f_1 - f_2)dE = \frac{2e^2}{h}V_{1-2}\int_{-\infty}^{\infty}\delta(E-\mu)dE = \frac{2e^2}{h}V_{1-2} = G_e^0 V_{1-2}, \tag{3}$$

where v has cancelled, resulting in a fundamental quantum of electronic conductance $G_e^0 = 2e^2/h$ that is independent of material properties [15,16]. This was experimentally verified in 1988, when quantized conductance steps were observed for current flow across point contacts made between continuum reservoirs [16]. Finite conductance, in the absence of scattering, results from resistances in the connections between the one-dimensional channel and each of the continuum reservoirs. Stronger coupling of the channel to the contacts increases the velocity of electron propagation through the junction, but proportionally reduces the density of states.

If an obstacle is present in the channel that transmits electrons with an energy-dependant probability $\tau(E)$, ranging from zero to one, then Eq. (3) is restated as

$$I_{1-2} = \frac{2e}{h}\int_{-\infty}^{\infty}\tau(E)(f_1 - f_2)dE, \tag{4}$$

for a small voltage difference between the contacts, this equation simplifies to

$$I_{1-2} = \frac{2e^2}{h}\tau(E)|_{E=\mu}V_{1-2} = G_e^0\tau(E)|_{E=\mu}V_{1-2} = G_e V_{1-2}, \tag{5}$$

where G_e represents the electronic conductance of a non-ideal channel, which is proportional to $\tau(E)$ at $E = \mu$ (for metallic contacts, $\mu = E_F$). Hence, a measurement of G_e amounts to a prediction of $\tau(E_F)$.

2.2. Thermoelectric properties

Inspection of the Landauer formula (Eq. (4)) suggests that an electric current will be induced by different reservoir temperatures if the transmission function is not constant in the region of the Fermi energy. A similar phenomenon is more intuitively described by the heating of an ideal gas, where hot ideal gas molecules move faster than cold ideal gas molecules. In the presence of a temperature gradient ΔT, a net diffusion of molecules from hot to cold occurs. In a closed system, this will result in a density gradient of the ideal gas. In metals the electrons resemble molecules in an ideal gas (except that they are fermions), and the charge density gradient from hot to cold results in an open-circuit voltage difference V. Asymmetries in mobilities and populations of hot ($E > \mu$) and cold electrons ($E < \mu$) cause this voltage difference, much like the asymmetry in speeds of the ideal gas molecules result in a density gradient. Thermopower S quantifies this transport property by relating ΔT and V as $V = -S\Delta T$. Thermopower is also a transport property of molecular junctions that can be experimentally measured, directly related to the transmission function, and utilized for energy conversion.

A relationship between S and $\tau(E)$ is needed to understand what types of junctions will have high thermoelectric performance, and to relate conductance measurements and thermopower measurements. This relationship was first developed by Butcher [17] and is derived by setting Eq. (4) equal to zero because S is defined at open circuit ($I_{1-2} = 0$). The occupation difference between the contacts $(f_1 - f_2)$ is expanded, with reference to contact 1, to account for differences in the electronic chemical potentials $\Delta\mu_{1-2}$ and temperatures ΔT_{1-2}

$$0 = \frac{2e}{h}\int_{-\infty}^{\infty}\tau(E)\left[\left(\left.\frac{\partial f}{d\mu}\right|_{\mu=\mu_1}\right)_{T_1}\Delta\mu_{1-2} + \left(\left.\frac{\partial f}{dT}\right|_{T=T_1}\right)_{\mu_1}\Delta T_{1-2}\right]dE. \tag{6}$$

The temperature derivative is then written in terms of energy $\partial f/\partial T = -T^{-1}(E-\mu)\partial f/\partial E$, and the chemical potential derivative is then approximated as $\partial f/\partial\mu = -\partial f/\partial E \approx \delta(E-\mu)$. The following relationship is determined after substitution of these expressions into Eq. (6)

$$\frac{\Delta\mu_{1-2}}{\Delta T_{1-2}} = \frac{1}{\tau(E)|_{E=\mu_1}}\int_{-\infty}^{\infty}\tau(E)\frac{(E-\mu_1)}{T_1}\frac{\partial f_1}{dE}dE. \tag{7}$$

The transmission function is then Taylor expanded $\tau(E) = \tau(E)|_{E=\mu_1} + (E-\mu_1)\partial\tau(E)/\partial E|_{E=\mu_1}$ which yields

$$\frac{\Delta\mu_{1-2}}{\Delta T_{1-2}} = \int_{-\infty}^{\infty} \frac{(E-\mu_1)}{T_1}\frac{\partial f_1}{dE}dE + \frac{1}{\tau(E)|_{E=\mu_1}}\left(\frac{\partial\tau(E)}{\partial E}\bigg|_{E=\mu_1}\right) \times \int_{-\infty}^{\infty} \frac{(E-\mu_1)^2}{T_1}\frac{\partial f_1}{dE}dE, \quad (8)$$

where the first integral is zero because it is symmetric about the chemical potential, and the second integral equals $\pi^2 k_B^2 T_1/3$ through the use of the Somerfeld expansion. The change in chemical potential results in an observed voltage, $\Delta\mu_{1-2} = -eV_{1-2}$

$$S = -\frac{V_{1-2}}{\Delta T_{1-2}} = -\frac{\pi^2 k_B^2 T}{3e}\left(\frac{1}{\tau(E)}\frac{\partial\tau(E)}{\partial E}\right)\bigg|_{E=\mu}. \quad (9)$$

Here $-V_{1-2}/\Delta T_{1-2}$ is by definition the thermopower of the junction, and the subscript 1 has been dropped from μ and T. Hence, the thermopower is related to the derivative of the transmission function at the chemical potential of the contacts (E_F for metal contacts) [17,18]. Intuitively, this parallels the qualitative result for bulk materials, because the derivative is a quantitative measure of the asymmetry between hot and cold electrons.

2.3. Quantum of thermal conductance

The thermoelectric figure of merit, ZT, is also related to thermal transport, which results from both electrons and phonons. In analogy to charge transport, thermal transport between equilibrium reservoirs can be described with the Landauer formalism. Both phonons and electrons contribute to the energy current $J_{1-2} = J_{1-2,p} + J_{1-2,e}$ and thermal conductance $G_{Th} = J_{1-2}/\Delta T_{1-2} = G_{Th,p} + G_{Th,e}$. For an ideal channel traversed by electrons and phonons, a limit exists to its thermal conductance, even in the absence of scattering mechanisms along its length. This quantum of thermal conductance is now derived for phonons (i.e. the $G^0_{Th,p}$).

The flow of energy from contact 1 to contact 2 due to phonons $J_{1-2,p}$ is written as a summation over all phonon modes indexed by wavevector k and polarization i

$$J_{1-2,p} = \sum_i \int_0^{\infty} \frac{dk}{2\pi}\hbar\omega_i(k)\,v_i(k)(n_1 - n_2), \quad (10)$$

where $\omega_i(k)$ and $v_i(k)$ are the phonon's frequency and group velocity, and n_1 and n_2 are the phonon occupation probabilities of contacts 1 and 2 (for phonons these are Bose-Einstein distributions $n_j = (e^{\hbar\omega_i/k_BT_j} - 1)^{-1}$). Conversion of Eq. (10) to an energy integral over $\hbar\omega_i$ results in a cancellation of velocity because $v_i(k) = \partial\omega_i/\partial k$

$$J_{1-2,p} = \sum_i \int_{\omega_i(0)}^{\infty} \frac{d\omega}{2\pi}\hbar\omega_i(n_1 - n_2). \quad (11)$$

Then $n_1 - n_2$ is then expanded for a small temperature difference between contacts 1 and 2 as,

$$n_1 - n_2 = \frac{\partial n}{\partial T}\Delta T_{1-2} = \frac{x_i e^{x_i}}{(e^{x_i}-1)^2}\frac{\Delta T_{1-2}}{T}, \quad (12)$$

where $x_i = \hbar\omega_i/k_BT$. The thermal conductance is found by substituting Eq. (12) into Eq. (11), and dividing both sides by ΔT_{1-2}

$$G_{Th,p} = \frac{J_{1-2,p}}{\Delta T_{1-2}} = \frac{k_B^2 T}{h}\sum_i \int_{x_i(0)}^{\infty} \frac{x_i^2 e^{x_i}}{(e^{x_i}-1)^2}dx_i. \quad (13)$$

At low temperatures, $G_{Th,p}$ of a single mode simplifies to $G^0_{Th,p} = k_B^2\pi^2 T/3h$, which is known as the fundamental quantum of thermal conductance [19,20]. Recent experiments have measured this quantum at low temperatures using nanostructured suspended dielectric bridges between thermal reservoirs [20]. If an obstacle is present in the channel, which transmits phonons with a frequency dependant probability $\tau_P(\omega_i)$ ranging from zero to one, then Eq. (11) is restated as

$$J_{1-2,p} = \sum_i \int_{\omega_i(0)}^{\infty} \frac{d\omega}{2\pi}\tau_P(\omega_i)\hbar\omega_i(n_1 - n_2). \quad (14)$$

The energy current due to electrons, based on the electronic transmission function, is

$$J_{1-2,e} = \frac{2}{h}\int_{-\infty}^{\infty}\tau(E)E(f_1 - f_2)dE, \quad (15)$$

and the electronic thermal conductance in an ideal channel results in $G^0_{Th,e} = 2k_B^2\pi^2 T/3h$, which is exactly twice that of phonons due to the electronic spin degeneracy of two. It is interesting to note that the quantum of thermal conductance is independent of carrier statistics, unlike electronic conductance [21,22].

2.4. Lorentzian transmission

The molecule acts as an obstacle in the conducting channel, and accurately representing its transmission function is of fundamental interest [15]. Transmission through the confined states of the organic molecule is defined by their alignment and coupling to delocalized states in the contacts. To first approximation, the electronic states in the contacts are connected to the mth molecular orbital by two tunneling barriers [23,24]. As depicted in Fig. 2C, these barriers describe the spatial gap between delocalized states in the contacts and bound states in the molecule. As a consequence, the transmission function $\tau(E)$ can be described by a two barrier resonant tunneling model that has resonant Lorentzian peaks (as presented in Ref. [23])

$$\tau_m(E) = \frac{4\Gamma_{m,1}\Gamma_{m,2}}{(\Gamma_{m,1} + \Gamma_{m,2})^2 + 4(E - E_m)^2}, \quad (16)$$

where the resonant energy levels are related to the molecular orbital energy levels, and $\Gamma_{m,1} + \Gamma_{m,2}$ is the broadening of these discrete orbitals due to their finite lifetime as a double barrier bound state. Total transmission can then be written in terms of a summation of transmission through all the participating orbitals

$$\tau(E) = \sum_{m=1}^{M}\tau_m(E), \quad (17)$$

where the frontier orbitals (i.e., HOMO and LUMO) dominate transport in a molecular junction. By substituting Eq. (16) into Eqs. (5) and (9) we find that the electronic conductance and thermopower based on a Lorentzian peaks are

$$G_e = \frac{2e^2}{h}\tau(E)|_{E=\mu} \quad S = \sum_{m=1}^{M}\frac{\pi^2 k_B^2 T}{3e}\frac{2(\mu - E_m)\tau_m(\mu)}{\Gamma_{m,1}\Gamma_{m,2}}. \quad (18)$$

The Lorentzian form defined by Eq. (18) will be used to qualitatively understand the implications of our experimental results throughout this article. A sample Lorentzian based transmission function, and the associated thermopower, are plotted in Fig. 3A and B. Lorentzian peaks are accurate representations of $\tau(E)$ if (i) the density of states in the contacts is constant and (ii) weakly coupled to the molecular orbitals [24]. While these conditions are not strictly met in real molecular junctions, the Lorentzian form has been substantiated by more rigorous calculations [25,26], and is a useful tool for analysis and prediction [27,28].

Alternatives to the Lorentzian transmission function, having either more or less complexity have been proposed to describe electronic transport in molecular junctions. A simpler approach is the Simmons rectangular tunneling barrier model, which was originally developed for describing electronic transport across

dielectric layers. The Simmons model has been extensively used to describe the exponential decay of electronic conductance with molecular length, but more recent studies suggest that it is inadequate for describing trends in thermopower [27] and transition voltage spectroscopy [29]. More rigorous approaches typically use density functional theory (DFT) to self-consistently determine junction electronic structure and electrostatic potential profiles. Transport properties are then evaluated from the Landauer formula using a transmission function evaluated within a Green's function (GF) formalism [24]. Over the past decade significant progress has been made in extending these techniques to create predictions of transmission that agree with experiments. In the following sections, experimental progress in the measurement of electronic conductance and thermopower will be discussed. In parallel, the relevant theoretical work that has been used to guide or explain these studies will be presented – though our coverage of theory is not intended to be exhaustive. The relevant theory has been recently reviewed by Galperin et al. [30,31].

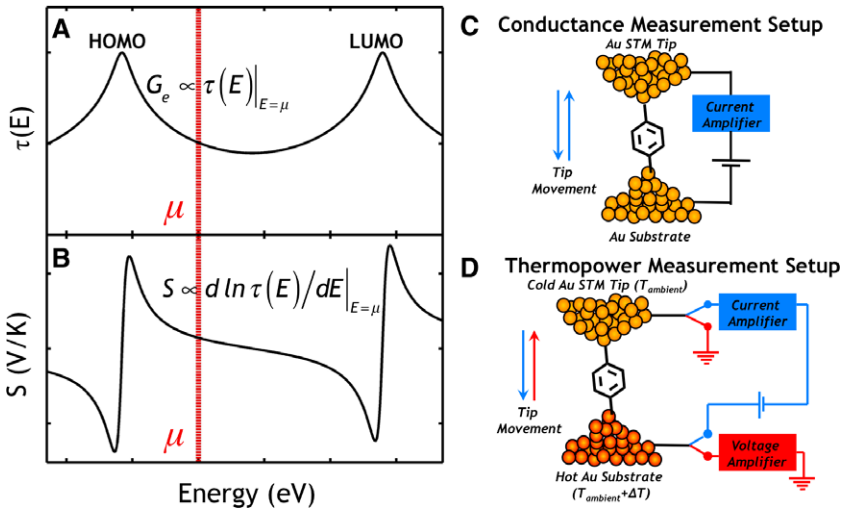

Fig. 3. Conductance and thermopower related to transmission. (A) Example of an electronic transmission function $\tau(E)$ where μ is shown closer to the HOMO. Low bias conductance G_e is related to the magnitude of $\tau(E)$ at μ. (B) Thermopower S is related to the slope of $\ln\tau(E)$ at μ. For a HOMO dominated molecule $S > 0$. (C) STM-break junction technique for measurement of electronic conductance. As the STM tip is withdrawn from the substrate steps in measured current can be used to infer the conductance of single molecules bridging the electrodes. (D) STM-break junction technique for measurement of thermopower. As the tip approaches the substrate a voltage bias is applied, and current is monitored to determine when a molecular junction has been created. Once a junction is present, the voltage bias is removed and the open-circuit voltage due to the thermopower of the junction is measured using a voltage amplifier.

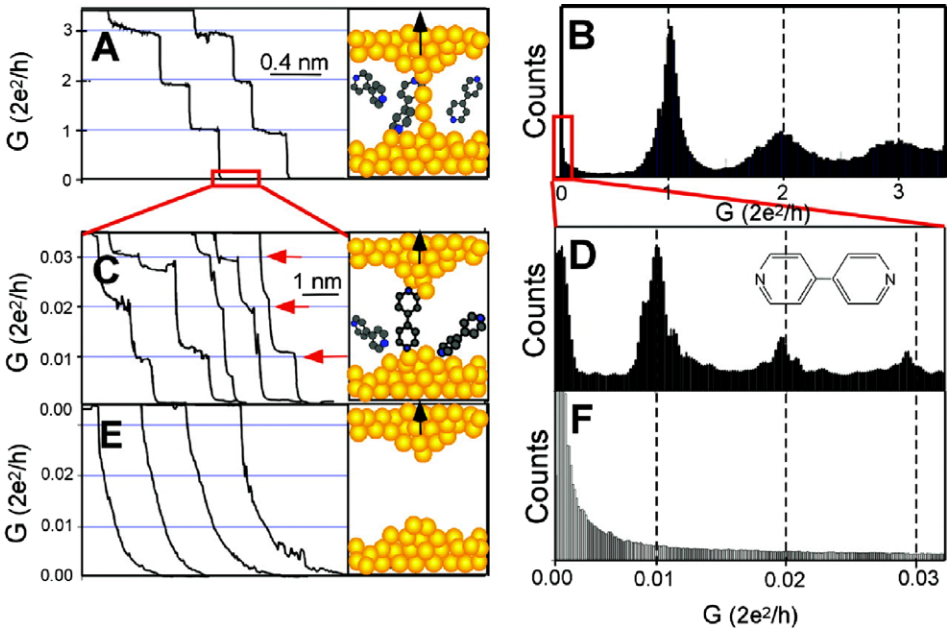

Fig. 4. Schematic of an STM-break junction and conductance data. (A) Conductance of Au–Au point contacts formed between a Au STM tip and a Au substrate decreases in quantum steps of $G_e^0 = 2e^2/h$ as the tip was withdrawn from the substrate. (B) Corresponding conductance histograms built from step heights have peaks at $1\,G_e^0$, $2\,G_e^0$, and $3\,G_e^0$. (C) As the tip was further withdrawn a series of lower conductance steps appeared when 4,4′-bipyridine molecules were present in the surrounding toluene solution. (D) Corresponding conductance histograms built from lower conductance steps have peaks near $0.01\,G_e^0$, $0.02\,G_e^0$, and $0.03\,G_e^0$, that are attributed to one, two, and three molecules. (E and F) In the absence of molecules, conductance steps were not observed. From Xu et al. [66], reprinted with permission from AAAS.

2.5. Experimental measurement techniques of conductance in molecular junctions

Reed's initial measurements of electronic conductance of single-molecule junctions [6] inspired a surge of molecular conductance measurement techniques. Though single-molecule junctions offered the ability to measure one molecule's conductance, many considered the junctions difficult to characterize and experimentally challenging to create [32]. In particular, these measurements are clouded by difficulties in verifying the number of molecules in a given junction and statistical difficulties in separating the expected variations in molecular junction properties from experimental artifacts. As an alternative, measurements of self-assembled monolayers (SAMs) have served as a basis to understand molecular conductance. In these measurements, a collection of molecular junctions (electrically in parallel) are created by trapping SAMs between a variety of metal contacts, including liquid Hg, metal-coated atomic force microscope (AFM) tips, and cross-wire junctions. Since many junctions are studied at once, these measurements represent an ensemble average and are most useful in comparing properties from one SAM to another in terms of structure-property relationships. In this case, reproducibility of the SAM-electrode interface is crucial. Typically, the SAM is formed atop a smooth metal surface which acts as the first contact. Deposition of a second contact on top of a SAM has been performed [33,34] but fabricating systems free of pin-holes between top and bottom electrodes is challenging [35–37].

Frequently, it is therefore advantageous to add a compliant top contact via physical means. For example, liquid Hg contacts demonstrate $I-V$ characteristics with transmission that decays exponentially with molecular length, as expected [32,38,39]. Similarly, the SAM may be contacted with a metal-coated atomic force microscope tip and measurements performed via conductive probe-atomic force microscopy (CP-AFM) [40–42]. This series of experiments conducted on hundreds of molecules at a time, is particularly useful in elucidating structure-property relationships such as the role of contact resistance (by measuring a series of alkane SAMs of increasing length and extrapolating to resistance at zero molecular length) or the transition from tunneling-type transport to a hopping regime via with increasing length of a series of conjugated molecules [40–45]. This technique uses a relatively small contact area so that as few as 100 molecules compose the parallel junction. An innovative alternative was proposed by Kushmerick et al. who created junctions using a cross-wire technique where a SAM was formed on one wire while another was kept bare [46]. The crossed wires were carefully brought together to create a metal–molecule–metal junctions by a Lorentz force in the presence of an E-field. This cross-wire technique has since been used to study symmetric and asymmetric molecules [46], the scaling of SAM measurements with number of molecules [47], $I-V$ behavior [48], and switching [49]. Furthermore, $I-V$ behaviors observed by both CP-AFM and cross-wire techniques exhibit a transition from direct tunneling to field emission that is clearly defined by an inflection point on the plot of $\ln(I/V^2)$ vs. $1/V$ [48]. This transition voltage can be related to the offset between μ and the nearest orbital, as demonstrated for a number of π-conjugated thiol molecules. This technique, known as transition voltage spectroscopy (TVS), has been used to understand the dependence of orbital offset on molecular conjugation and length [45,50].

Although SAM measurements allow access to ensemble properties, the lack of ensemble averaging in single-molecule experiments allows for sensitivity to contact geometry, orbital hybridization, and intermolecular interactions. Single-molecule experiments also represent a reasonable platform to compare theory and experiment because the systems are sufficiently simple to model using atomistic calculations. Hence, single-molecule experiments provide additional details crucial to transport processes, having both scientific intrigue and practical importance.

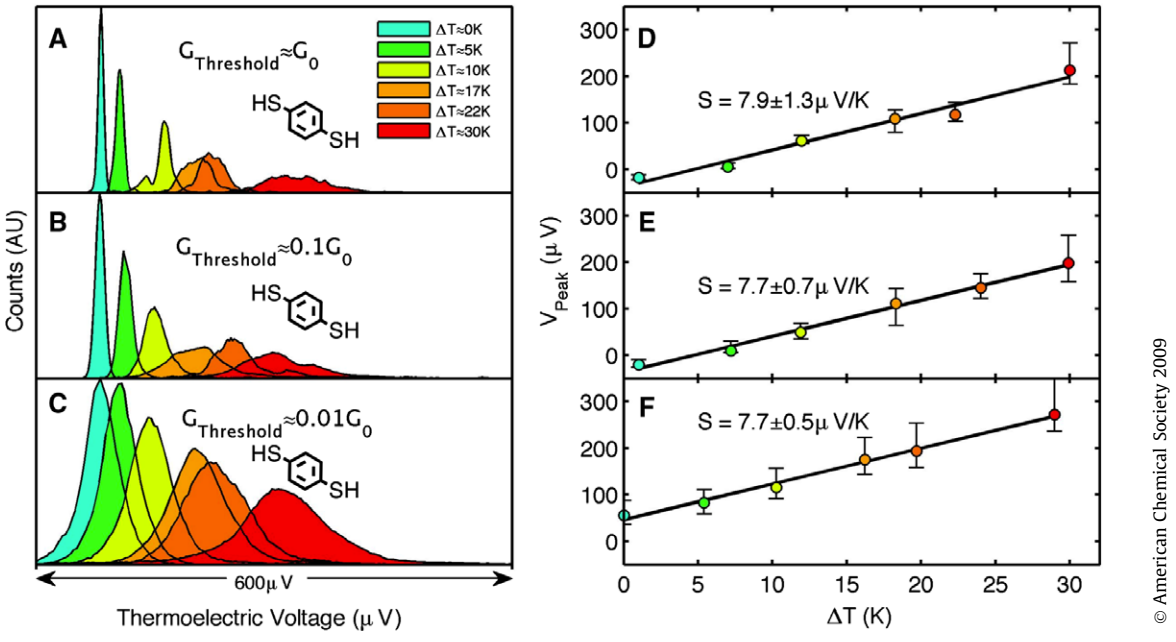

Fig. 5. Thermoelectric Voltage Histograms and linear fits for various threshold conductances. Thermopower is an intensive property and is therefore independent of the number of molecules in the junction. Conductance was used to identify the creation of a molecular junction. The STM tip approached the sample until this threshold conductance was reached, signifying the formation of a molecular junction. Once the junction formed, the STM tip was withdrawn and a switch replaced the voltage bias and current amplifier, with a voltage amplifier that measured the induced thermoelectric voltage. The threshold conductance determined the number of molecules present in the junction, at the point at which the thermoelectric voltage was measured; higher threshold conductance results in more molecules in the junction. Threshold conductances of $1G_0$, $0.1G_0$, and $0.01G_0$ were considered. Panels A–C show voltage histograms for Au–PDT–Au junctions with threshold conductances of (A) G_0, (B) $0.1G_0$, and (C) $0.01G_0$. Adapted with permission from Malen et al. [27]. Histogram peaks are plotted as a function of ΔT in panels D–F, and found to linearly increase. The slopes ($S = V_{peak}/\Delta T$) and 95% confidence intervals of the fit lines yield $S = 7.9 \pm 1.3$, 7.7 ± 0.7, and 7.7 ± 0.5 for threshold conductances of G_0, $0.1G_0$, and $0.01G_0$. These results are consistent with prior thermopower measurements of Au–PDT–Au junctions [8,28] and confirm that thermopower is an intensive property of molecular junctions.

Conductance and $I-V$ characteristics of single-molecule junctions have been extensively investigated by trapping molecules in break junctions formed by mechanical strain [6,51,52], electromigration [53–55], and scanning tunneling microscopes (STMs) [25,56–66]. Electromigration in thin metal wires creates gaps on the order of ~1 nm. When treated with a very dilute solution of molecules, occasionally single molecules or small groupings will bridge the gap allowing for electrical characterization. The stability of electromigrated break junctions (EMBJ) allows for $I-V$ sweeps, in comparison to mechanically controlled and STM-based break junctions which are not long-lasting enough for this type of characterization. Furthermore, a gate electrode can be incorporated in this architecture and allows for the positioning of the molecular orbitals with regard to the chemical potential of the contacts [12]. Kondo effects [67], single electron addition energies, and vibronic fine structure [68] have all been studied with this technique. Although EMBJ's have demonstrated immense utility, fabrication challenges and low yields result in an inability to accumulate significant statistics.

Mechanically controlled and STM-break junctions can be repeatedly broken and reformed in a short period of time so that a statistically significant sample set (1000s of data points) can be generated. Such junctions are formed when initially unified metallic contacts are mechanically separated until a ~1 nm gap is formed. In both cases, spatial precision is achieved by piezoelectric actuation and appropriate position feedback controls (e.g., tunneling current sensing or linear voltage differential transducers). Molecules present on the surface of the contacts (or within the surrounding medium) bridge the gap for electronic characterization.

Observation of quantized changes in the conductance of the junction, during the contact separation process, have been used to identify the single molecule electronic conductance. A schematic of the STM-break junction and related conductance data, from Xu et al. [66], are shown and described in Fig. 4. Current is monitored as the metallic contacts are separated. Initially unified metallic contacts are pulled into chains of gold atoms before completely breaking. The current decreases in integer multiples of G_e^0 during this stage in the withdrawal because integer transmission pathways exist in the gold chains, each dictated by Eq. (3). When the chains of gold atoms sever, it is possible for molecules to span the newly formed gap. A secondary set of steps with lower conductance appears in the subsequent stages of the current vs. distance profile. These steps are believed to come at integer multiples of the molecular conductance because multiple molecules initially bridge the gap in parallel, but fall off discretely until a single molecule remains momentarily. Conductance of the molecules G_e is some fraction of G_e^0, determined by $\tau(E)$ of the junction, as described in Eqs. (4) and (5). While some groups have observed steps at up to three integer multiples of G_e [65,66], others see only a single step at lower conductance attributable to the molecule [25,57–63]. Statistics are built by breaking and reforming the junction thousands of times, and grouping the measured conductance step heights into histograms. Histogram peaks represent the most frequently observed molecular conductance and histogram full width at half maximums (FWHMs) represent a variation in the observed conductance.

Recently, STM junctions of increased stability for $I-V$ characterization have also been formed by placing the subject molecule into an insulating host SAM and labeling it with a Au nanoparticle easily detectable by the STM tip [69]. Conductance switching [49] and electronic rectification [70] have been studied in this orientation. Gating can also be introduced in this orientation by performing the experiment within an electrolyte with controllable potential, (i.e., electrochemical gating) [71–74]. Because of its

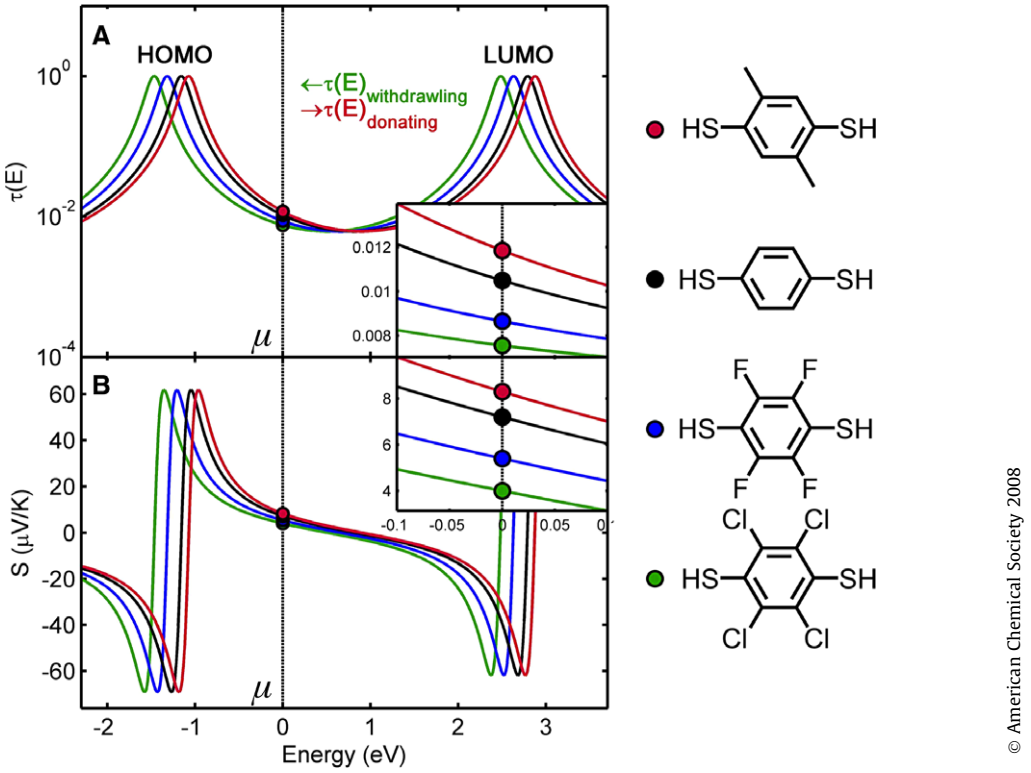

Fig. 6. Relation between the measured thermopower (S) of substituted Au–PDT–Au junctions to the position of μ. (A) Theoretical prediction [26] of the transmission function of a Au–PDT–Au junction plotted as a function of the offset between μ and the HOMO and LUMO. It is assumed that the transmission function has the same shape for the substituted molecules, but it is shifted with respect to μ. (B) The predicted thermopower of the junctions as a function of the relative position of the μ with respect to the HOMO and LUMO levels. The HOMO and LUMO are shifted relative to μ such that the predicted thermopower crosses μ at the measured value of S. When the measured value of $S_{\text{Au-BDT 4Cl-Au}} = +4 \pm 0.6$ (green band), $S_{\text{Au-BDT 4F-Au}} = +5.4 \pm 0.4$ (blue band), $S_{\text{Au-BDT-Au}} = +7.2 \pm 0.2$ (black band) and $S_{\text{Au-BDT 2Me-Au}} = +8.3 \pm 0.3$ (red band) are used in this figure, it is clear that the $G_e = \tau(E) * G_0$ is $\sim 0.008G_0$, $0.009G_0$, $0.011G_0$ and $0.012G_0$ respectively. Reprinted with permission from Baheti et al. [28].

repeatability, the STM-break junction technique has been widely used for measurements of both conductance and thermopower, and will be the focus of our detailed discussion that follows.

2.6. Conductance results lead to new open questions

Initial single-molecule conductance experiments focused on Au–PDT–Au junctions due to the robust Au–thiol bond, and conjugation that promised a conductive interconnect for molecular electronics. Despite the seemingly robust thiol bond, measurements of the low voltage conductance of PDT by the STM-break junction technique yielded vastly different values than were initially put forth by Reed's mechanical break junction; $1.1 \times 10^{-2} G_0$ compared to $6 \times 10^{-4} G_0$ [6,65]. Related experiments by Weiss and Lindsay observed real-time variations in the apparent height of thiol bound phenylene–ethenylene oligomers and long chain alkanes, as measured by STM [75,76]. They proposed that variations were caused by fluctuations in the molecule-substrate hybridization, likely caused by the Au–thiol bond. In parallel to the experimental work, a considerable computational effort aimed at understanding charge transport in single-molecule junctions predicted an even broader range of conductances for Au–PDT–Au junctions than was experimentally observed [77–83].

The microscopic details of the Au–thiol bond, not only caused debate about the magnitude and variations of conduction, but also whether transport is dominated by the HOMO or the LUMO of the molecule. From Eqs. (16) and (17), it is clear that the energy level most well aligned with the chemical potential of the contacts (E_F for Au contacts) will dominate transport. TVS can yield a quantitative prediction of this orbital's position relative to E_F when a bias is applied across the junction, but can't conclusively identify which orbital it is [84] and how it may be shifted from its zero bias

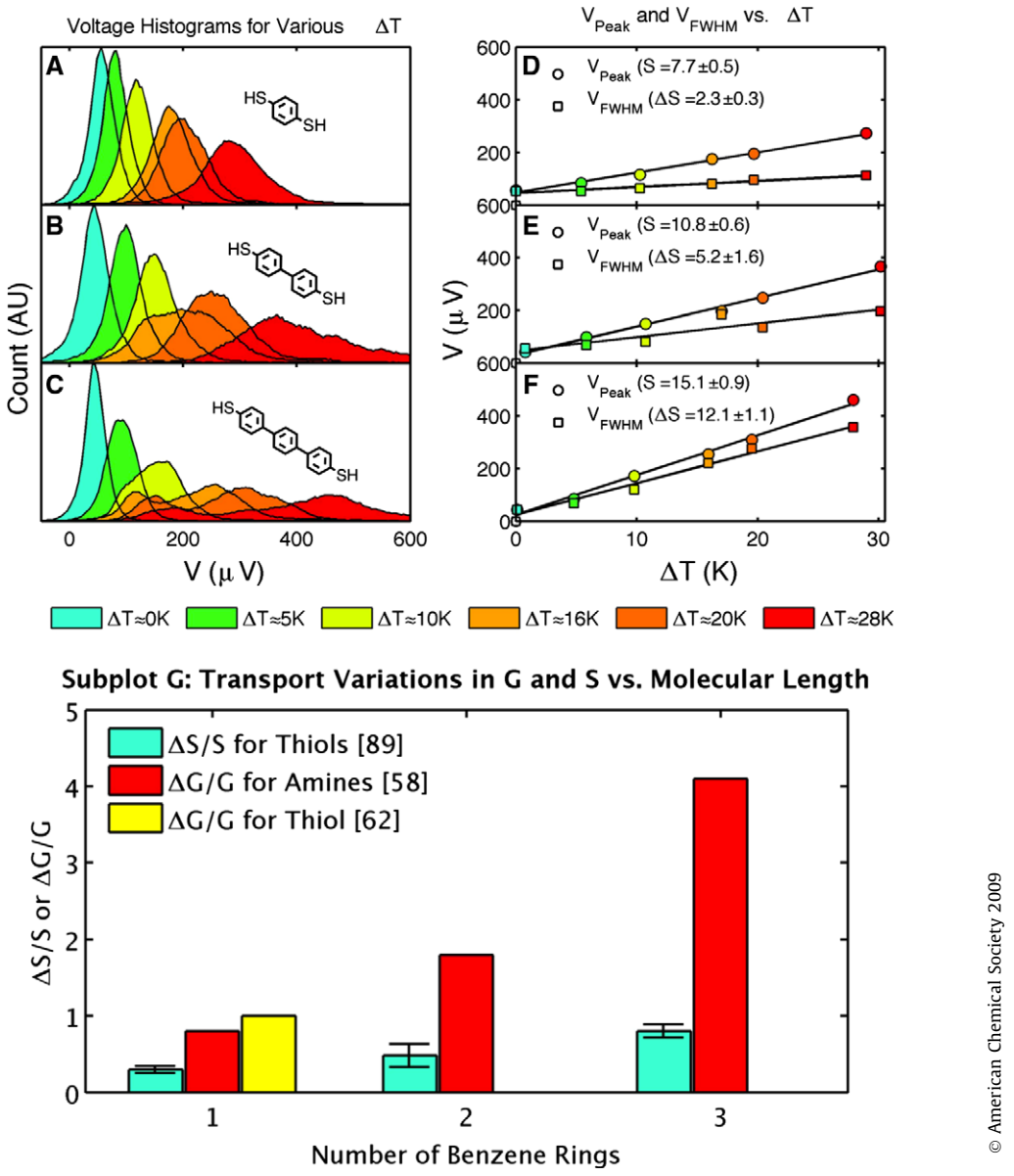

Fig. 7. Transport variations in molecular junctions. Panels A–C show voltage histograms from thermopower measurements of Au–PDT–Au, Au-4,4′-diphenyldithiol, and 4,4′-triphenyldithiol. Panels D–F show the histogram peaks (V_{peak}) and full width at half maximums (V_{FWHM}) plotted as a function of ΔT. The slope of V_{peak} vs. ΔT is S, while the slope in V_{FWHM} vs. ΔT represents a variation in S. $\Delta S/S$ from data shown in A–F and $\Delta G/G$ from earlier studies represent the normalized variability of thermopower and conductance measurements. Subplot G shows that $\Delta G/G$ increases with the number of phenyl rings for phenyldiamines [61], and $\Delta S/S$ increases with the number of phenyl rings for phenyldithiols. $\Delta G/G$ for the characteristically well defined conductance histograms of Au–phenyldiamine–Au junctions is larger than $\Delta S/S$ for the widely variable Au–phenyldithiol–Au junctions because S is less sensitive to electrode coupling as described by Eqs. (21) and (22). In part with permission from Malen et al. [92].

position. In the case of PDT, some groups contended that E_F of the contacts lies closer to the HOMO, while other groups contended that E_F lies closer to the LUMO [18]. Conductance measurements, in the absence of a gate, cannot identify the dominant molecular orbital because contributions from each orbital are perceived equivalently as current. By analogy, two point probe measurements of conductance in semiconducting crystals cannot distinguish between electron transport through the conduction band or hole transport through the valance band.

Length dependant behavior of the orbital offset and contact coupling are also irreconcilable with conventional conductance measurements alone. Both SAM and single molecule measurements show that the conductance of metal–molecule–metal junctions decays exponentially with molecular length. The simplest interpretation of length dependant conductance data suggests that the molecules behave like a rectangular tunneling barrier with a fixed and discrete height [44]. Theory indicates that this is an oversimplified picture since orbital energies depend on molecular length and the discrete levels broaden due to coupling with the contacts [85].

Substantial progress in conductance measurement and theory has been made over the past decade, but this work revealed new questions about the nature of electronic transmission that cannot be accessed from this simple set of measurements: (i) Which orbital dominates transmission in a given molecular junction and can its position be tuned by changing the chemistry of the junction? (ii) What is the nature of variations in thiol bound junctions? and (iii) Do molecules simply behave like tunneling barriers as the length dependence of conductance indicates, or is there more a complex behavior?

2.7. Thermopower in molecular junctions

Molecular thermopower measurements are performed using a modified STM setup in analogy to conductance measurements except that a temperature bias, instead of a voltage bias, is applied between the contacts [8]. The conductance measurement setup and thermopower measurement setup are compared in Fig. 3C and D. Subject molecules are dissolved in toluene and dropcast onto a gold-coated mica substrate. Evaporation of the solvent leaves the molecules bound to the gold surface. A resistance heater is used to heat the substrate to ΔT above ambient temperature, while the Au STM tip is maintained at ambient temperature. Initially the STM tip is driven towards the substrate. During this approach stage a voltage bias is applied between the tip and substrate. Current is monitored to determine when a molecular junction has been created. Once a threshold conductance is exceeded, the tip is motion is reversed. Simultaneously, the voltage bias is removed and the open-circuit voltage due to the thermopower of the junction is measured using a voltage amplifier. Like STM based conductance measurements, statistics are captured by consecutive repetitions of this approach-withdrawal sequence. Roughly 500–1000 junctions are formed at each ΔT for ΔT ranging between 0 and 30 K. Histograms are built from the data at each ΔT, without preselection. When the histogram peaks V_{peak} are plotted against ΔT, they form a straight line with a slope equal to the thermopower of the junction, (i.e., $S = V_{peak}/\Delta T$). The histograms and linear fits for PDT are shown in Fig. 5, for three threshold conductances.

Unlike conductance measurements, thermopower is an intensive property, and is insensitive to the number of molecules in the junction. Fig. 5 shows voltage histograms for PDT, taken at threshold conductances of $1G_0$, $0.1G_0$, and $0.01G_0$ [27]. The threshold conductance determines the number of molecules in the junction, at the point at which the thermoelectric voltage is measured; higher threshold conductance results in more molecules in the junction. The slopes and 95% confidence intervals of the fit lines yield $S = 7.9 \pm 1.3$, 7.7 ± 0.7, and 7.7 ± 0.5 for threshold conductances of G_0, $0.1G_0$, and $0.01G_0$. Within experimental error these results are identical and consistent with prior thermopower measurements of 1,4-phenyldithiol [8,28]. This can be explained analytically using Eq. (9). The transmission of N parallel molecules is $N\tau(E)|_{E=\mu}$, resulting in multiplicative conductance, but constant thermopower as follows:

$$S_N = \frac{-\pi^2 k_B T}{3e}\left(\frac{1}{\cancel{N}\tau(E)}\frac{\partial \cancel{N}\tau(E)}{\partial E}\right)_{E=\mu} = S_1, \tag{19}$$

where the N cancels and $S_N = S_1$. Eq. (19) demonstrates that thermopower is independent of the number of molecules in the junction, just as it is an intensive property of bulk materials.

2.7.1. Identifying and tuning p- or n-type heterojunctions using thermopower

Since thermopower depends on the derivative of the natural log of the transmission function at the chemical potential, the sign of

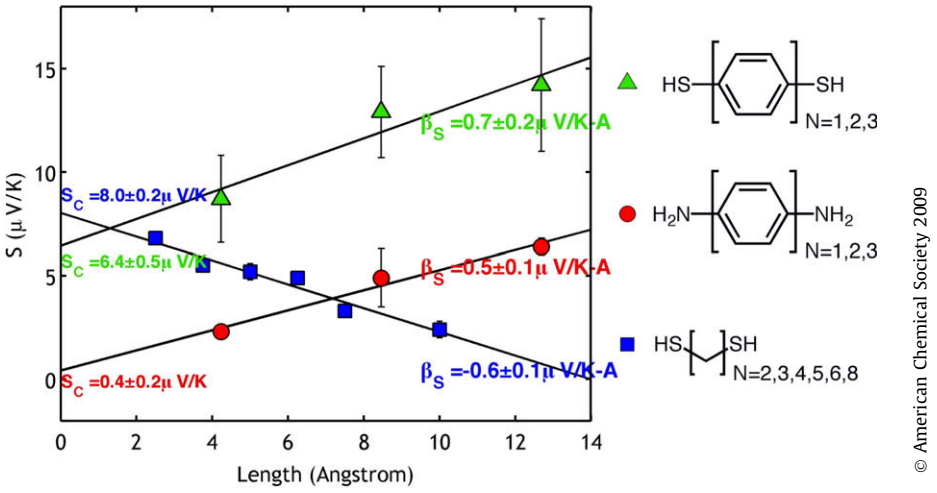

Fig. 8. Thermopower is plotted as a function of molecular length for N-unit phenylenedithiols ($N = 1, 2, 3$), phenylenediamines ($N = 1, 2, 3$), and alkanedithiols ($N = 2, 3, 4, 5, 6, 8$). Linear fits show that thermopower increases with length at a similar rate (β_S) for phenylenedithiols and phenylenediamines, while phenylenedithiols and alkanedithiols have a similar zero-length thermopower (S_C). These trends suggest that molecular backbone is related to β_S and the end group is related to S_C, in agreement with studies of conductance. Reprinted with permission from Malen et al. [27].

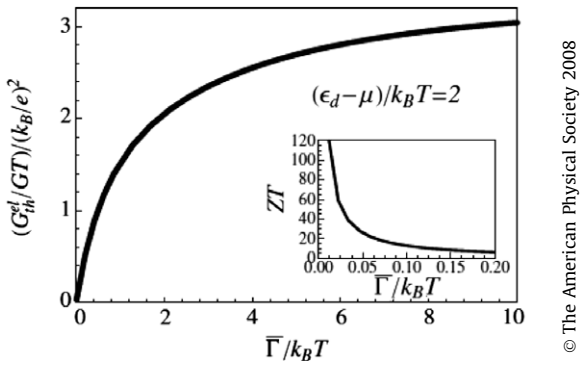

Fig. 9. The Lorenz number (main figure) and electronic ZT (inset) plotted as functions of $\Gamma/(k_BT)$, with $(E_i-\mu)/k_BT=2$ in both cases. Only the electron contribution to the thermal conductance is included. Note that the Lorenz number attains the Sommerfeld value of $\pi^2/3$ for $\Gamma \gg k_BT$ [100].

the thermopower is an unambiguous probe of the dominant transport orbital for molecules with smoothly varying transmission functions. Data from Fig. 5 shows that PDT has positive thermopower. Fig. 3 shows a hypothetical $\tau(E)$ in panel A, and the slope of its logarithm in panel B. A positive value of S results only when the μ is placed more closely to the HOMO. In the weak coupling limit, the Lorentzian approximation from Eq. (18) simplifies to

$$S \approx \sum_{m=1}^{M} \frac{\pi^2 k_B^2 T}{3e} \frac{2}{(\mu - E_m)}, \tag{20}$$

which demonstrates that thermopower will be dominated by the orbital (i.e., HOMO or LUMO) nearest the chemical potential. The sign will discriminate whether this orbital is higher or lower in energy than the chemical potential, therein identifying it as the LUMO or HOMO.

In practice, the measured value of S can be used to identify the position of μ relative to the molecular orbitals. While the sign of thermopower reveals the closest orbital, the magnitude of thermopower can provide quantitative insight to that orbital's position relative to the chemical potential, when the transmission function is well known. Paulsson and Datta suggested thermopower measurements expressly for this purpose [18]. Reddy and Jang's initial measurements on Au–PDT–Au junctions yielded positive thermopower and unambiguously identified the HOMO as the dominant transport orbital [8], suggesting thermopower's complementary diagnostic role to conductance measurements in characterizing molecular electronics.

The ability to predictably tune transport through chemical design is a universal advantage of organic electronics. For example, predictable shifts in the HOMO and LUMO levels of molecules can be realized through substitution of simple aromatic molecules. Similar tunability is possible in molecular junctions, where changes to the substituent groups shift the HOMO and LUMO relative to E_F, much like a gate contact. The role of substituent groups was systematically probed by measurements of conductance on phenylenediamines (PDAs) [63] and thermopower on PDTs [28]. Relative to the E_F of the contacts, electron-withdrawing substituents shifted the HOMO peak to higher energies (further from E_F) resulting in lower measured thermopowers and conductances, while electron donating groups shift the HOMO to lower energies (closer to E_F) resulting in higher thermopowers and conductances, as shown in Fig. 6 and predicted by a recent ab-initio study of thermopower [86].

2.7.2. Transport variations

Transport variations have caused a great deal of confusion and discouragement in the potential of molecular electronics. As circuits approach the sub-nanoscale, transport variations will overwhelm ensemble averages, and play a more critical role. Thiol's nonspecific binding to Au led some to believe that lingering discrepancies across conductance experiments were the result of contact geometry. In particular, it has been proposed that thiol bonded to an adatom, bridge, or hollow site on the Au surface the junction would possess very different transport properties [83,87–90]. Basch et al. found that conductance could vary by orders of magnitude when changing the overlap between the molecular π-orbitals and the s-like states near the Fermi level of the Au contacts [88]. For alkanedithiol molecules, Muller concurred that the zero-voltage conductance depends strongly on the details of the contact geometry [91]. Conductance measurements of thiol bound molecules have witnessed fluctuations in conductance [75,76], and discrepancies in the measured values and spread in conductance that are not well understood [60,62,65].

The breadth of the voltage histograms as a function of ΔT collected during a thermopower measurement can be used to gain insight to transport variations [92]. As shown in Fig. 7A–C, the breadth of each thermoelectric voltage histogram increases with increasing ΔT. In fact, the FWHM is plotted as a function of ΔT in Fig. 7D–F, and increases linearly. The slope of the fit is a measure of the thermopower variations, termed ΔS. These variations result from changes in the orbital offset and coupling to the continuum electrode states. For PDT, with the assumption of Lorentzian transmission it can be shown that $\Delta S/S$ is directly related to variations in the HOMO offset from the chemical potential ΔE_{HOMO}

$$\frac{\Delta S}{S} \approx \frac{\Delta E_{\mathrm{HOMO}}}{(\mu - E_{\mathrm{HOMO}})}, \tag{21}$$

where $\mu - E_{\mathrm{HOMO}}$ is the nominal offset. PDTs with one, two, and three rings were measured, and $\Delta S/S$ ranged from 0.3 to 0.84, implying variations in the HOMO offset similar in magnitude to the nominal offset itself [92]. Energy spans this large can result only from substantial fluctuations in the junction structure and local environment.

While the variation in thermopower defined in Eq. (21) is independent of $\Delta\Gamma$, the variation in conductance is not

$$\frac{\Delta G}{G} \approx \frac{\Delta\Gamma_{\mathrm{HOMO},1}}{\Gamma_{\mathrm{HOMO},1}} + \frac{\Delta\Gamma_{\mathrm{HOMO},2}}{\Gamma_{\mathrm{HOMO},2}} + \frac{2\Delta E_{\mathrm{HOMO}}}{(\mu - E_{\mathrm{HOMO}})}. \tag{22}$$

Hence, variations in the thermopower of PDT are large, but still dwarfed by the minimum reported variations in its conductance [65], which is $\Delta G/G \approx 1.0$ due to its dependence on $\Delta\Gamma$.

Venkataraman and coworker's conductance results for phenylenes with endgroups other than thiol indicate that thiols are particularly sensitive to contact geometry and orbital hybridization. In particular, conductance histograms built from thousands of measurements had a more well defined peak for amine endgroups than for thiol endgroups, due to the specificity of the Au–amine bond [62]. Theorists soon agreed with these conclusions. Li suggests that amines have a very specific bonding geometry, that does not become distorted during the evolution of a stretching junction resulting in a well defined conductance [93]. Quek et al. computed the conductance of PDA with reasonable accuracy and found it to be comparatively insensitive to contact geometry [25]. Furthermore, Quek et al. used the results of the PDA experiments as a benchmark to demonstrate the limitations of DFT calculations for computing the conductance of molecular junctions. Applying approximate self-energy corrections to the PDA transmission function revealed large corrections to DFT orbital energies that ultimately resulted in reasonable agreement with experimental work.

Perhaps the most interesting trend in the variations is their propensity to increase with molecular length. $\Delta S/S$ of PDT increases with increasing molecular length [92] in agreement trends in con-

ductance variations ($\Delta G/G$) of the PDAs [61]. Fig. 7G summarizes these measurements of $\Delta G/G$ and $\Delta S/S$. Comparison of several molecules indicates that the observed thermopower distributions are caused by variations in contact geometry, orbital hybridization, and intermolecular interactions – all of which increase with molecular length [92]. High frequency thermal fluctuations were ruled out as a source of the observed variations in thermopower due to the limited bandwidth of the measurement setup.

2.7.3. Length dependence

The length dependence of observable properties in molecular junctions is an indication of the physics underlying transport. Complementary measurements of conductance and thermopower reveal length dependant trends in orbital alignment and contact coupling. Length dependence has been probed in both saturated molecules with C–C σ-bonds and conjugated molecules with delocalized π-electrons. Short alkane chains (<10 CH_2 units) are the prototypical saturated molecules, and have been studied with a range of endgroups including thiols and amines. Experiments have found that their electronic conductance decays exponentially with molecular length L,

$$G_e = G_e^C \exp(-\beta_G L), \tag{23}$$

where β_G is the decay constant and G_e^C is the zero length extrapolated contact conductance. Several groups have found $\beta_G \sim 0.9$ Å^{-1}, independent of measurement technique, endgroup or contact material [42,44,57,62]. Both CP-AFM and STM measurements of short polyaromatic molecules (<3 phenyl rings) with delocalized π-electrons and smaller HOMO–LUMO gaps yield smaller values of $\beta_G \sim 0.4$ Å^{-1}, also independent of endgroup or contact material [42,61]. In contrast, extrapolated values of G_e^C are independent of saturated or conjugated backbone, and similar for molecules having the same endgroups and contact materials [42–44].

Measurements of thermopower for a series of phenylenes and alkanes with varying binding groups corroborate the conductance trends [27]. The data, shown in Fig. 8, suggest that thermopower changes linearly with molecular length [8,27],

$$S = \beta_S L + S_C, \tag{24}$$

where β_S is the slope that depends backbone chemistry, and S_C is the zero length extrapolated thermopower that depends on end-group and contact material, in good agreement with predictions. Although in agreement with more complex theory [85], these thermopower trends cannot be explained by a simple rectangular tunneling barrier model (i.e., the Simmons model). Inconsistencies of the rectangular tunneling barrier model were also posited by Huisman when comparisons were made to data from TVS [29]. Instead, complimentary thermopower and conductance data were fit to the Lorentzian model derived in Eq. (16), revealing length dependant trends in the HOMO alignment ($\mu - E_{\mathrm{HOMO}}$) and contact coupling (Γ_{HOMO}). Specifically, transport is HOMO dominated and as molecular length increases the HOMO aligns closer to the Fermi energy of the contacts as $\mu - E_{\mathrm{HOMO}}\tilde{L}^{-1}$, but becomes more decoupled from them as $\Gamma_{\mathrm{HOMO}} \sim e^{-L}$. In contrast, β_S for alkanedithiols suggests that transmission is largely affected by gold-sulfur metal induced gap states residing between the HOMO and LUMO.

3. Outlook on molecular heterojunctions as the building blocks of thermoelectric materials

Junction thermopower measurements provide insight into the electronic structure of the molecular junction, but also bear on an as-yet the unexplored field of thermoelectric energy conversion in hybrid materials. Sharply peaked density of states at the organic–inorganic interface mimic the single energy level transport envisioned by Mahan and Sofo to optimize ZT [9]. While S and σ are primarily based on electronic structure, k has both electron and phonon contributions. In bulk materials S and σ are opposing functions of doping concentration, and a compromise that optimizes $S^2\sigma$ is sought. Without jeopardizing this compromise, incremental gains to ZT have been recently realized through reductions in the phonon contribution to k [94–96]. In search of greater gains in ZT, S and σ can be concurrently optimized in molecular junctions where the organic molecular orbitals (MOs) are well aligned with the chemical potential of the contacts [28].

Electronic properties of bulk materials can be formulated using the Boltzmann transport equation, which defines the electronic conductivity as a function of the chemical potential

$$\sigma(\mu) = e\gamma(\mu)n(\mu) = e\gamma(\mu)\left[\frac{2}{3}\mu D(\mu)\right], \tag{25}$$

where e is the electron charge, $\gamma(\mu)$ is the carrier mobility, $n(\mu)$ is the carrier density (bracketed quantity), and $D(\mu)$ is the density of states at μ. Intuitively, Eq. (25) shows that σ can be increased by either (i) increasing the carrier density, or (ii) increasing the carrier mobility. Thermopower is related to these properties using Mott's formula [97–99] for thermopower as

$$\begin{aligned} S(\mu) &= -\frac{\pi^2 k_B^2 T}{3e}\frac{d\ln\sigma(E)}{dE}\bigg|_{E=\mu} \\ &= -\frac{\pi^2 k_B^2 T}{3e}\left(\frac{d\ln n(E)}{dE}\bigg|_{E=\mu} + \frac{d\ln\gamma(E)}{dE}\bigg|_{E=\mu}\right), \end{aligned} \tag{26}$$

which demonstrates the dependence of S on the energy derivative of the carrier density and carrier mobility at μ. Eq. (26) shows that the magnitude of $S(\mu)$ can be increased by increasing the energy dependence of either (i) $n(E)$ or (ii) $\gamma(E)$ at μ. Doping a material is perhaps the easiest way to significantly change $n(E)$, but for a parabolic band structure ($D(\mu) \propto \sqrt{\mu}$) this has opposing effects on σ and S. As the material is doped, μ, $n(\mu)$, and $\sigma(\mu)$ increase, while $d\ln n(E)/dE|_{E=\mu}$ and $S(\mu)$ decrease. This opposing response to doping is the mathematical result when the curvature of $\ln n(E)$ is negative ($d^2\ln n(E)/\,dE^2|_{E=\mu} < 0$).

Are there bulk materials that have a positive curvature of $\ln n(E)$? Heremans et al. successfully answered this question in inorganic materials by exploiting a distortion in the density of states of lead telluride due to the formation of thallium impurity levels [98]. The curvature of this distortion permitted doubling of σ at high temperatures without affecting S. We now suggest taking this idea one step further by considering transport through a single MO. Mahan and Sofo have already shown mathematically that ZT is optimized for electronic transport through a single energy level [9]. Metal–molecule–metal junctions retain the molecular character as the effective $D(E)$ in the junction has sharp peaks related to the molecular orbital energies. The curvature in the vicinity of this energy level is ideal for thermoelectric energy conversion. Using the simple Lorentzian model and the assumption that $G_eT/G_{th,e} \approx 3e^2/k_B^2\pi^2$ (one divided by the Lorentz number, further discussed in the following paragraph), we can arrive at the following simple expression for ZT of the ith molecular orbital

$$Z_iT = \frac{S^2 G_e T}{G_{th,p} + G_{th,e}} = \frac{S^2 G_e T}{G_{th,e}(1+R)} \approx \frac{4\pi^2 k_B^2 T^2/3}{(\mu - E_i)^2(1+R)}, \tag{27}$$

where R is the ratio of the phonon thermal conductance to the electron thermal conductance and S has been substituted from Eq. (20). This expression shows that as the $\mu - E_i$ decreases, ZT rapidly increases. The challenge becomes selecting a molecule-contact system where the MOs are well aligned with μ of the contacts.

The promise of optimized ZT for single level transport, and the observation of single molecule thermopower, sparked recent theo-

retical interest in high ZT molecular junctions. Though Eq. (28) proves that ZT increases as the MOs are more closely aligned with μ, various authors have made quantitative estimates of ZT. Murphy et al. showed that weakly coupled molecular junctions can operate close to the Carnot efficiency if the molecular orbital is of order k_BT from μ of the electrodes [100]. In this case, ZT is limited by phonon contributions to the thermal conductance, and the largest possible $ZT \sim (G_{Th}^{Ph}/G_{Th}^{0})^{-1/2}$. Fig. 9 has been reproduced from Murphy's study, and shows that when the coupling between the molecular orbital and the contacts is weak, and the MOs are well aligned with μ, extremely high ZT can result. Liu et al., Finch et al. show giant thermopower and ZT can be attained by molecules exhibiting Fano resonances in the region of the μ [101]. Their calculations indicate that for molecules with sidegroups, $\tau(E)$ can be dramatically modified by Fano resonances that can be predictably tuned to coincide with μ. Ke et al., make calculations of S for several real molecules and find that it reaches values in excess of 100 μV/K for large molecules when the μ is well aligned with the MOs. Bergfield and Stafford suggest that S for molecular junctions will reach a temperature-independent value of $\pm\pi k_B/e\sqrt{3} \approx \pm 156$ μV/K [102], which is competitive with S of various inorganic thermoelectric materials, and an order of magnitude larger than any existing organic molecule measurements. A separate challenge revolves around the design of scalable materials system that incorporate large numbers of molecular junctions to satisfy energy generation requirements. For example, a scalable concept material composed of arrays of polyacetylene molecular junctions with n-doped silicon nanoparticles was studied by Muller. In agreement with single molecule studies, Muller's material exhibited high ZT values for sufficiently small phonon contributions to the thermal conductance [103].

Though predictions of ZT are promising, several questions remain. Perhaps the most open question is: What is the thermal conductance of molecular junctions? Only a few experiments and little theory have addressed this transport property which has contributions from both electrons and phonons. Wang's et al. experiments are most relevant as they measured the thermal conductance of alkanedithiol SAMs sandwiched between a GaAs substrate and a Au film [11]. Wang found that the thermal conductances ($\sim$30 MW/m^2-K) were comparable to the lowest thermal interface conductances on record, and independent of alkane length for 8, 9, and 10 CH_2 units. Wang et al. studied heat flow in alkanemonothiol SAMs on Au surfaces using femtosecond laser pulses to heat the backside of the Au surface [104]. Conductance rates were interpreted from the arrival time of the vibrations' leading edge at the molecules' opposite ends that caused thermal disorder detectable by vibrational spectroscopy. The authors found that heat flow was limited by the Au–molecule interface, traveled ballistically along the chains (at a velocity of 1 km/s), and resulted in a length independent molecular conductance of 50 pW/K-molecule.

Galperin et al. recently reviewed theoretical studies of vibrational effects [31] and introduced a non-equilibrium Green's function-based approach to describe heat conduction in molecular junctions [30]. In agreement with Wang's experimental observations, Galperin predicts that thermal conductivity will be independent of length, at room temperature, where all vibrational modes are populated. Paradoxically, at low temperature only the low frequency phonon modes that exist in longer molecules will be populated, and heat conductance should be inversely proportional to molecular length. An alternative study of ZT in molecular junctions found that a characteristic temperature exists which marks the transition from electron to phonon dominated thermal conductance [105]. In alkanedithiols this temperature is predicted to be less than 10 K indicating that phonon contributions are crucial at room temperature. Vibronic coupling, resulting from inelastic interactions between vibrations and electrons, has been probed experimentally by inelastic tunneling spectroscopy (IETS) [106,107]. IETS allows one to probe the active vibrational states due to changes in the electronic conductance, but cannot describe the rate at which these vibrations transport energy through the junction. Further experiments regarding the nature and mechanism of thermal transport in molecular-junctions are necessary to clarify the effects of molecular endgroups, conjugation, and length as well as to explore the roll of the contacts and separate electron and phonon contributions. Such evidence is also necessary to accurately determine the thermoelectric figure of merit ZT for the organic–inorganic heterojunctions.

4. Conclusions

The frontiers of energy conversion sit at the interface between organic and inorganic materials. Molecular heterojunctions are a platform that can be used to closely study this interface, and have already received extensive attention for molecular electronics. We have herein reviewed the progress in the field of molecular electronics, concentrating on new findings relevant to thermoelectric energy conversion and transport from the last 5 years. Experimentally, Tao's development of an STM-break junction technique in 2003 prompted statistical studies of single-molecule conductance that have improved confidence in its measurement [66]. In 2007, Reddy used a similar STM technique to study thermopower in molecular junctions which has since lead to several complimentary studies of electronic transport [8,27,28,92]. Theoretical studies have made significant progress by making corrections to DFT based Landauer approaches and more accurately depicting the contact geometry of molecular junctions. In some cases, quantitative agreement between theory and experiment has been possible for predictions of both conductance and thermopower.

While thermopower has been a useful diagnostic that compliments conductance measurements, it has also led to studies of thermoelectric energy conversion in molecular junctions. Further investigation of single-molecule thermal transport and thermopower are needed to scope the feasibility of thermoelectric energy conversion in molecular junctions. First, limited attention has been given to heat transport in molecular junctions. More specifically, very little data on the thermal conductance of molecular junctions exists. Furthermore, a tool to study single molecule heat transport has not yet been introduced, and a universal technique for measurement of SAM thermal properties is not agreed upon. Second, thermoelectric conversion in molecular junctions can be expanded. Although initial thermopower studies have yielded new information about electronic transport, there is little experimental progress towards efficient thermoelectric conversion in molecular junctions. Studies of larger molecules, with smaller bandgaps or degenerate molecular orbitals may yield concurrently enhanced S and G_e by improving the likelihood that an MO will be well aligned with the chemical potential of the contacts. So far, only metals with inherently low thermopowers have been used as contacts. An improvement in ZT may be realized by using semiconducting contacts that already have high thermopowers.

Acknowledgments

This work was supported by the DOE-BES Thermoelectrics program at Lawrence Berkeley National Laboratories. SKY would also like to gratefully acknowledge a fellowship from the John and Fannie Hertz Foundation and J.A.M. would like to acknowledge the National Defense Science and Engineering Graduate Fellowship. We would also like to thank Dr. Jeffrey Neaton, Peter Doak, and Profes-

sor Pramod Sangi Reddy for the many thought inspiring conversations about this field.

References

[1] A.L. Briseno et al., Nature 444 (7121) (2006) 913.
[2] S.R. Forrest, Nature 428 (6986) (2004) 911.
[3] E.V. Shevchenko et al., Nature 439 (7072) (2006) 55.
[4] A. Aviram, M.A. Ratner, Chem. Phys. Lett. 29 (2) (1974) 277.
[5] D.M. Adams et al., J. Phys. Chem. B 107 (28) (2003) 6668.
[6] M.A. Reed et al., Science 278 (5336) (1997) 252.
[7] C. Joachim, M.A. Ratner, Proc. Natl Acad. Sci. USA 102 (25) (2005) 8801.
[8] P. Reddy et al., Science 315 (5818) (2007) 1568.
[9] G.D. Mahan, J.O. Sofo, Proc. Natl Acad. Sci. USA 93 (15) (1996) 7436.
[10] T.E. Humphrey, H. Linke, Phys. Rev. Lett. 94 (9) (2005).
[11] R.Y. Wang, R.A. Segalman, A. Majumdar, Appl. Phys. Lett. 89 (17) (2006).
[12] K. Moth-Poulsen, T. Bjornholm, Nat. Nanotechnol. 4 (9) (2009) 551.
[13] A. Nitzan, M.A. Ratner, Science 300 (5624) (2003) 1384.
[14] N.J. Tao, Nat. Nanotechnol. 1 (3) (2006) 173.
[15] Y. Imry, R. Landauer, Rev. Mod. Phys. 71 (2) (1999) S306.
[16] B.J. Vanwees et al., Phys. Rev. Lett. 60 (9) (1988) 848.
[17] P.N. Butcher, J. Phys.: Condens. Matter 2 (22) (1990) 4869.
[18] M. Paulsson, S. Datta, Phys. Rev. B 67 (24) (2003) 241403.
[19] D.E. Angelescu, M.C. Cross, M.L. Roukes, Superlattices Microstruct. 23 (3–4) (1998) 673.
[20] K. Schwab et al., Nature 404 (6781) (2000) 974.
[21] L.G.C. Rego, G. Kirczenow, Phys. Rev. B 59 (20) (1999) 13080.
[22] I.V. Krive, E.R. Mucciolo, Phys. Rev. B 60 (3) (1999) 1429.
[23] C. Kittel, P. McEuen, Introduction to Solid State Physics, vol. xix, eighth ed., J. Wiley, Hoboken, NJ (p. 680)
[24] S. Datta, Quantum Transport: Atom to Transistor, vol. xiv, Cambridge University Press, Cambridge, UK, New York, 2005. p. 404.
[25] S.Y. Quek et al., Nano Lett. 7 (11) (2007) 3477.
[26] M. Paulsson, S. Datta, Phys. Rev. B 67 (24) (2003).
[27] J.A. Malen et al., Nano Lett. 9 (3) (2009) 1164.
[28] K. Baheti et al., Nano Lett. 8 (2) (2008) 715.
[29] E.H. Huisman et al., Nano Letters 9 (2009) 3909.
[30] M. Galperin, A. Nitzan, M.A. Ratner, Phys. Rev. B 75 (15) (2007).
[31] M. Galperin, M.A. Ratner, A. Nitzan, J. Phys.: Condens. Matter 19 (10) (2007).
[32] R.E. Holmlin et al., J. Am. Chem. Soc. 123 (21) (2001) 5075.
[33] J.R. Heath, M.A. Ratner, Phys. Today 56 (5) (2003) 43.
[34] Y. Luo et al., ChemPhysChem 3 (6) (2002) 519.
[35] J.G. Brown, R.D. Blanton, J. Electron. Test.: Theory Appl. 23 (2–3) (2007) 131.
[36] Y. Chen et al., Nanotechnology 14 (4) (2003) 462.
[37] K.T. Shimizu et al., Adv. Mater. 18 (12) (2006) 1499.
[38] M.A. Rampi, G.M. Whitesides, Chem. Phys. 281 (2–3) (2002) 373.
[39] K. Slowinski, H.K.Y. Fong, M. Majda, J. Am. Chem. Soc. 121 (31) (1999) 7257.
[40] D.J. Wold, C.D. Frisbie, J. Am. Chem. Soc. 122 (12) (2000) 2970.
[41] D.J. Wold, C.D. Frisbie, J. Am. Chem. Soc. 123 (23) (2001) 5549.
[42] D.J. Wold et al., J. Phys. Chem. B 106 (11) (2002) 2813.
[43] J.M. Beebe et al., J. Am. Chem. Soc. 124 (38) (2002) 11268.
[44] V.B. Engelkes, J.M. Beebe, C.D. Frisbie, J. Am. Chem. Soc. 126 (43) (2004) 14287.
[45] S.H. Choi, B. Kim, C.D. Frisbie, Science 320 (5882) (2008) 1482.
[46] J.G. Kushmerick et al., Phys. Rev. Lett. 89 (8) (2002).
[47] J.G. Kushmerick et al., Nano Lett. 3 (7) (2003) 897.
[48] J.M. Beebe et al., Phys. Rev. Lett. 97 (2) (2006).
[49] A.S. Blum et al., Nat. Mater. 4 (2) (2005) 167.
[50] J.M. Beebe et al., ACS Nano 2 (5) (2008) 827.
[51] E. Lortscher, H.B. Weber, H. Riel, Phys. Rev. Lett. 98 (17) (2007).
[52] S.M. Wu et al., Nat. Nanotechnol. 3 (9) (2008) 569.
[53] Z.K. Keane et al., Nano Lett. 6 (7) (2006) 1518.
[54] H. Park et al., Nature 407 (6800) (2000) 57.
[55] J. Park et al., Nature 417 (6890) (2002) 722.
[56] J. Hihath et al., Nano Lett. 8 (6) (2008) 1673.
[57] S.Y. Jang et al., Nano Lett. 6 (10) (2006) 2362.
[58] M. Kamenetska et al., Phys. Rev. Lett. 102 (126803) (2009).
[59] S.Y. Quek et al., Nat. Nanotechnol. 4 (4) (2009) 230.
[60] J. Ulrich et al., J. Phys. Chem. B 110 (6) (2006) 2462.
[61] L. Venkataraman et al., Nature 442 (7105) (2006) 904.
[62] L. Venkataraman et al., Nano Lett. 6 (3) (2006) 458.
[63] L. Venkataraman et al., Nano Lett. 7 (2) (2007) 502.
[64] J.L. Xia, I. Diez-Perez, N.J. Tao, Nano Lett. 8 (7) (2008) 1960.
[65] X.Y. Xiao, B.Q. Xu, N.J. Tao, Nano Lett. 4 (2) (2004) 267.
[66] B.Q. Xu, N.J.J. Tao, Science 301 (5637) (2003) 1221.
[67] W.J. Liang et al., Nature 417 (6890) (2002) 725.
[68] E.A. Osorio et al., Adv. Mater. 19 (2) (2007) 281.
[69] X.D. Cui et al., Science 294 (5542) (2001) 571.
[70] G.M. Morales et al., J. Am. Chem. Soc. 127 (30) (2005) 10456.
[71] N.J. Tao, Phys. Rev. Lett. 76 (21) (1996) 4066.
[72] T. Albrecht et al., J. Am. Chem. Soc. 128 (20) (2006) 6574.
[73] F. Chen et al., Nano Lett. 5 (3) (2005) 503.
[74] A. Nitzan et al., J. Phys. Chem. B 104 (24) (2000) 5661.
[75] Z.J. Donhauser et al., Science 292 (5525) (2001) 2303.
[76] G.K. Ramachandran et al., Science 300 (5624) (2003) 1413.
[77] A.M. Bratkovsky, P.E. Kornilovitch, Phys. Rev. B 67 (11) (2003) 115307.
[78] M. Di Ventra, S.T. Pantelides, N.D. Lang, Phys. Rev. Lett. 84 (5) (2000) 979.
[79] E.G. Emberly, G. Kirczenow, Phys. Rev. B 58 (16) (1998) 10911.
[80] L.E. Hall et al., J. Chem. Phys. 112 (3) (2000) 1510.
[81] S.H. Ke, H.U. Baranger, W.T. Yang, J. Chem. Phys. 123 (11) (2005) 114701.
[82] S.H. Ke, H.U. Baranger, W.T. Yang, J. Chem. Phys. 122 (7) (2005) 074704.
[83] K. Stokbro et al., Comput. Mater. Sci. 27 (1–2) (2003) 151.
[84] A. Tan, S. Seid, P. Reddy, Appl. Phys. Lett. 96 (2010) 013110.
[85] S.Y. Quek et al., Nano Lett. 9 (11) (2009) 3949.
[86] S.H. Ke et al., Nano Lett. 9 (3) (2009) 1011.
[87] Y.Q. Xue, M.A. Ratner, Phys. Rev. B 68 (11) (2003).
[88] H. Basch, R. Cohen, M.A. Ratner, Nano Lett. 5 (9) (2005) 1668.
[89] S.H. Ke, H.U. Baranger, W.T. Yang, J. Chem. Phys. 123 (11) (2005).
[90] S.H. Ke, H.U. Baranger, W.T. Yang, J. Chem. Phys. 122 (7) (2005).
[91] K.H. Muller, Phys. Rev. B 73 (4) (2006).
[92] J.A. Malen et al., Nano Lett. 9 (10) (2009) 3406.
[93] Z. Li, D.S. Kosov, Phys. Rev. B 76 (3) (2007).
[94] T.C. Harman et al., Science 297 (5590) (2002) 2229.
[95] K.F. Hsu et al., Science 303 (5659) (2004) 818.
[96] R. Venkatasubramanian et al., Nature 413 (6856) (2001) 597.
[97] M. Cutler, N.F. Mott, Phys. Rev. 181 (3) (1969) 1336.
[98] J.P. Heremans et al., Science 321 (5888) (2008) 554.
[99] M. Jonson, G.D. Mahan, Phys. Rev. B 21 (10) (1980) 4223.
[100] P. Murphy, S. Mukerjee, J. Moore, Phys. Rev. B 78 (16) (2008).
[101] C.M. Finch et al., J. Phys.: Condens. Matter 20 (2) (2008).
[102] J.P. Bergfield, C.A. Stafford, Nano Lett. 9 (8) (2009) 3072.
[103] K.H. Muller, J. Chem. Phys. 129 (4) (2008).
[104] Z.H. Wang et al., Science 317 (5839) (2007) 787.
[105] Y.S. Liu, Y.R. Chen, Y.C. Chen, ACS Nano 3 (11) (2009) 3497.
[106] J.G. Kushmerick et al., Nano Lett. 4 (4) (2004) 639.
[107] W.Y. Wang et al., Nano Lett. 4 (4) (2004) 643.

Glossary of terms and symbols

D(E): electronic density of states
DFT: density functional theory
e: positive unit of charge
E_F: electronic Fermi energy
f: Fermi Dirac distribution
G_e^0: fundamental quantum of electronic conductance
G_e: electronic conductance
G_{Th}^0: fundamental quantum of thermal conductance
G_{Th}: thermal conductance
Γ: Lorentzian peak parameter
HOMO: highest occupied molecular orbital
I: electronic current
IETS: inelastic tunneling spectroscopy
J: heat current
k: thermal conductivity
LUMO: lowest unoccupied molecular orbital
γ: electron mobility
μ: chemical potential (Fermi energy in a metal)
ω: phonon frequency
S: thermopower (Seebeck coefficient)
σ: electronic conductivity
SAM: self-assembled monolayer
T: temperature
TDDFT: time dependent density functional theory
$\tau(E)$: transmission function
V: voltage bias
v: velocity
ZT: thermoelectric figure of merit

Jonathan A. Malen is currently an Assistant Professor in the Mechanical Engineering Department at Carnegie Mellon University. Malen earned a B.S. in Mechanical Engineering from the University of Michigan (2000), an S.M. in Nuclear Engineering from the Massachusetts Institute of Technology (2003), and a Ph.D. in Mechanical Engineering from the University of California, Berkeley (2009) before joining Carnegie Mellon in 2009. While at UCBerkeley he was a National Defense Science and Engineering Graduate Fellow. His research expertise is experimental measurement of thermal energy transport and conversion in organic–inorganic heterostructures and nanostructured semiconductors.

Shannon Yee received a B.S. in Mechanical Engineering (2007) and M.S. in Nuclear Engineering (2008) from The Ohio State University. In 2007, he was recognized as a US Department of Energy Advanced Fuel Cycle Initiative fellow and collaborated with Idaho National Laboratory on transmutation and recycled nuclear fuel for his M.S. work. In 2008, he was awarded a John and Fannie Hertz Foundation fellowship to pursue further studies and he is currently pursuing his Ph.D. at the University of California, Berkeley where he is working on transport and energy conversion in nanoscale systems.

Arun Majumdar received a B.Tech in Mechanical Engineering from the Indian Institute of Technology, Bombay in 1985, and a Ph.D. in Mechanical Engineering from UC, Berkeley in 1989. He is a member of the National Academy of Engineering and has held faculty appointments at Arizona State University (1989–1992), UC, Santa Barbara (1992–1996), and most recently at UC, Berkeley (1996–2009). While at Berkeley, Majumdar also held the role of Associate Laboratory Director for Energy and Environment at the Lawrence Berkeley National Laboratory. In 2009, President Barack Obama appointed him as the first Director of ARPA-E within the Department of Energy.

Rachel A. Segalman is an Associate Professor of Chemical Engineering at UC, Berkeley and an Associate Faculty Scientist at Lawrence Berkeley National Laboratories. Segalman earned a B.S. in Chemical Engineering at UT, Austin and a Ph.D. in Chemical Engineering at UC, Santa Barbara. Since her arrival to Berkeley in 2004, Segalman has recieved the NSF CAREER award, TR35, PECASE, and Alfred P. Sloan Fellowship. Her research expertise in polymeric materials includes functional block copolymers, conjugated rod-coil block copolymers, and polymers and nanocomposites for thermoelectric applications. She has also developed expertise in the measurement of structure-property relationships in molecular junctions.